HEAT TRANSFER CHARACTERISTICS OF TWO-PHASE He I (4.2 K) THERMOSIPHON FLOW

L. Benkheira[1], B. Baudouy[1*] and M. Souhar[2]

[1]DAPNIA, SACM-LCSE
CEA – Centre de Saclay
91191 Gif-Sur-Yvette Cedex, France
[2]Laboratoire d'Énergétique et de Mécanique Théorique et Appliquée
LEMTA – ENSEM, CNRS UMR 7563
2, avenue de la forêt de Haye – B.P. 160
54504 VANDOEUVRE Cedex, France

ABSTRACT

In the framework of the cryogenic cooling system design of a large superconducting magnet under construction at CERN-Geneva, heat transfer in two-phase He I natural circulation loop has been investigated experimentally. The experiments were conducted on a 2 m thermosiphon loop with copper tube of 10 mm inner diameter uniformly heated over a length of 0.95 m. All data were obtained near atmospheric pressure. Evolution of the exit vapour quality and wall superheat as a function of heat flux are presented and analyzed. A comparison between the two phase heat transfer coefficient h_{TP} determined in our study and the most relevant correlations available in literature is made. Further, we predict h_{TP} with a correlation based on the combining effects of forced convection and nucleate boiling by a power-type asymptotic model. Finally, we present the boiling crisis study and we propose a critical heat flux correlation as a function of channel height to diameter ratio (*z/D*) to model our experimental results.

Keywords : Thermosiphon, two-phase flow, helium, h_{TP}, CHF

* Corresponding author. Tel.: +331 69 08 42 07; Fax: +331 69 08 69 29 E-mail address: bertrand.baudouy@cea.fr

NOMENCLATURE

C_p: liquid specific heat
D: diameter
F: amplification factor
g: gravitational acceleration
G: mass velocity
h: heat transfer coefficient
i: liquid enthalpy
L: channel length
L_v: latent heat of vaporization
LHe: liquid helium
$\dot{m}$: mass flow rate
q: heat flux
q_{cr}: critical heat flux
S: suppression factor
T: temperature
x: vapour quality
z: channel height

Greek symbols
α: void fraction
μ: dynamic viscosity
ρ: density
σ: surface tension
λ: thermal conductivity

Dimensionless numbers
Fr: Froude number $= G^2 / \rho_f^2 gD$
Ku: Kutateladze number $= q_{cr} / \sqrt{\rho_v} L_v \sqrt[4]{\sigma g (\rho_f - \rho_v)}$
Pe: Peclet number $= GDC_p / \lambda$
p_r: reduced pressure $= p / p_c$
Pr: Prandtl number $= C_p \mu / \lambda$
Re: Reynolds number $= GD / \mu$
Y: a parameter in Shah's correlation $= PeFr^{0.4} (\mu_f / \mu_v)^{0.6}$
We_f: Weber number $= G^2 L_v / \rho_f$

Subscripts
c: critical state
cr: critical heat flux
cv: forced convection
e: exit
EN: nucleate boiling
f: liquid phase
i: inlet
sat: saturated state
sub: subcooled state
t: total
TP: two-phase
v: vapour phase
w: wall

1 INTRODUCTION

Low temperature superconducting materials widely used in the construction of high magnetic field coils must be cooled down to liquid helium temperature. For magnet operating at 4.2 K, three refrigeration techniques are mainly employed based on: pool cooling where the superconducting coil is entirely submerged in a large volume of stagnant liquid, two-phase forced convection where the flow is created by a pressurization system such as low temperature centrifugal mechanical pumps and two-phase natural convection where the flow is driven by voids. The last cooling technique is interesting because it eliminates the use of pumps which requires a costly maintenance and operation at low temperatures. In view of this, it has been planned, at CEA-Saclay, to cool down the 4 Tesla Compact Muon Solenoid (CMS) magnet with a two-phase natural circulation loop [1]. CMS is one of the high-energy physics particles detectors dedicated to the Large Hadron Collider (LHC) experiment under construction at CERN, Geneva. The magnet consists of five independent modules, each of them cooled indirectly through a network of aluminium tubes soldered on the magnet casing. The modules are supplied with liquid helium via a downward tube from a phase separator that serves also as a reservoir.

Understanding natural two-phase flow phenomena in liquid helium and the ability to predict heat transfer characteristics are of great importance for design purpose in such cooling system. Unfortunately, literature survey reveals that a majority of thermosiphon boiling vertical two-phase flow studies concerned with non-cryogenic fluids [2], especially water, and only a few experimental works are available on He I two-phase natural circulation. To the best of our knowledge, Mollard and Johannes performed a study on a square cross-section tubes having hydraulic diameter of around 8 mm with aspect ratio comprised between 10 and 110 [3]. Scarce data on the subject and the LHC project opportunity have motivated our laboratory to carry out experiments to highlight the thermo-hydraulic characteristics of He I natural boiling flow. Previous results have shown, up to a vapour quality of 20%, that the evolution of the total mass flow rate and the tube pressure drop with the heat flux is similar to classical fluids and the two-phase heat transfer coefficient can be predicted with an acceptable accuracy by the homogeneous model and Martinelli's correlation [4, 5].

Heat transfer in flow boiling is governed by both forced convection and nucleate boiling mechanisms. Hence, empirical correlations developed to estimate the heat transfer coefficient attempt to take in account the combined effect of the macro-convection associated with the bulk mass flow and the nucleate boiling considering the liquid motion (micro convective agitation) behind a departing bubble from the wall. They can be classified depending on the contribution from each mechanism. Rohsenow and Clark [6] have suggested that the total wall heat flux is given by adding the effects of forced convection and nucleate boiling,

$$q = h_{CV}\left(T_w - T_f\right) + q_{EN}\,, \tag{1}$$

where T_w and T_f are, respectively, the wall and fluid temperatures, h_{CV} is the forced convection heat transfer coefficient computed from an appropriate non-boiling correlation as that proposed by Dittus-Boelter [7] and q_{EN} is the pool boiling heat flux given by Rohsenow's correlation [8]. More recent work by Bergles and Rohsenow indicates that forced convection fully developed nucleate boiling data cannot be predicted by that of saturated pool boiling because of the bulk flow influence on wall nucleation [9]. This suggests that the superposition method of Eq. (1) should be used with some precaution. Later, alternative methods to account the coupling effect of vapour bubbles and the bulk liquid flow have been proposed by several authors, where the heat transfer coefficient in two-phase flow, h_{TP} is described by:

$$h_{TP} = \left(\left(F.h_{CV,fo}\right)^n + \left(S.h_{pool}\right)^n\right)^{1/n}, \tag{2}$$

where $h_{CV,fo}$ is the forced convection heat transfer coefficient based on the liquid mass flow rate and h_{pool} is the nucleate boiling heat transfer coefficient associated to the pool boiling configuration. F is the amplification coefficient introduced to take into account the increase of convective turbulence

due to the presence of the vapour phase. *S* is the suppression coefficient stemming from the decrease of nucleation in forced convection compared to pool boiling conditions due to a thinner boundary layer. n is an exponent that expresses the degree of interaction between the forced convection and the nucleate boiling processes. A number of flow boiling correlations published so far are based on Eq. (2) such as those proposed by Chen [10], Shah [11], Winterton and co-workers [12, 13], Kandlikar [14] and Steiner *et al.* [15]. However, most of them are based on non-cryogenic liquid data and are only reliable for conditions very close to experiments from where they originate.
The present study, an experimental investigation into heat and mass transfer in a two-phase thermosiphon flow of helium at low temperature (4.2 K), has the primary objective to provide helium boiling flow data for mass flow rates, wall temperature distribution, heat transfer coefficient and critical heat flux. Secondly, this study aims to study flow regimes through the heat transfer coefficient analysis. Lastly, we evaluate the existing correlations for heat transfer coefficient and critical heat flux and develop correlations based on our data.

2 EXPERIMENTAL SET-UP AND PROCEDURE

2.1 Experimental Set-up

As shown in Fig. 1, the experimental facility consists of a vertical oriented two meter long cryostat insulated by vacuum space and a liquid nitrogen shield to minimize radiation and conduction heat transfer from the outside ambient and an the insert containing the thermosiphon loop elements needed for the study. The loop is mainly composed of two vertical tubes joined in a U shape with the upper ends connected to the liquid-vapour phase separator. The 0.3 m high separator has a diameter of 0.45 m and serves as a liquid reservoir for the experiment. It is provided with a superconducting liquid level sensor, Cryomagnetics LM-500 with a ±1 mm resolution, a 20 W heater, a Germanium thermometer and an absolute pressure gauge PTres to monitor liquid temperature and pressure inside phase separator. Thermal barriers are composed of two sets of radiation shields. The first one, made of aluminium, entirely covers the separator, the test section and the downward tubing and it is cooled down by helium vapour flowing out of the separator during the operation. The second is made of two copper horizontal shields. The downward tube has a diameter of 40 mm. The test section is made of CuA1 tube (RRR=145) with 10 mm inner diameter and 1 mm wall thickness. The thermal conductivity at 4.2 K of the A1 class copper is 958 W/m.K, which insures isothermal heating. A numerical simulation of the copper tube with the stainless steel connectors has been performed with commercial software [16]. The simulation considered that the tube and the connectors are in contact internally with the two phase mixture modeled with single phase flow at 4.2 K in the center and a heat transfer coefficient at the walls. On the other side, the tube and the connectors are considered isolated since they are in a vacuum environment. The heater with its real twist pitch is also modeled. The calculation has been performed from 100 W/m^2 to 2000 W/m^2 with a heat transfer coefficient corresponding to the experimental value at the given heat flux. For the entire range of heat flux, the temperature difference within the copper tube thickness is lower than 510^{-4} K, which is lower than the sensitivity of the thermometers used and the heat flux through the connector is null since the temperature gradient is null. The test section is heated along 95 cm with a riser, *i.e.* an unheated part, of 50 cm. The wall heater (9 Ω at 4.2 K) is made of manganin resistance wire wrapped around the copper tube with a twist pitch of 10 mm to create homogeneous heat dissipation. It is placed in a groove of 0.75 mm depth, covered with epoxy resin, DP190, with a thermal conductivity of 0.02 W/m.K at 4.2 K. The heat flux is known within few percent. The tube is wrapped with several layers of aluminised Mylar super-insulation to minimize radiation heat transfer losses with surroundings.
Five Germanium thermometers (model GR-200-A-2500) distributed along the tube were used for measurement of local inner wall temperature to deduce the corresponding heat transfer coefficient

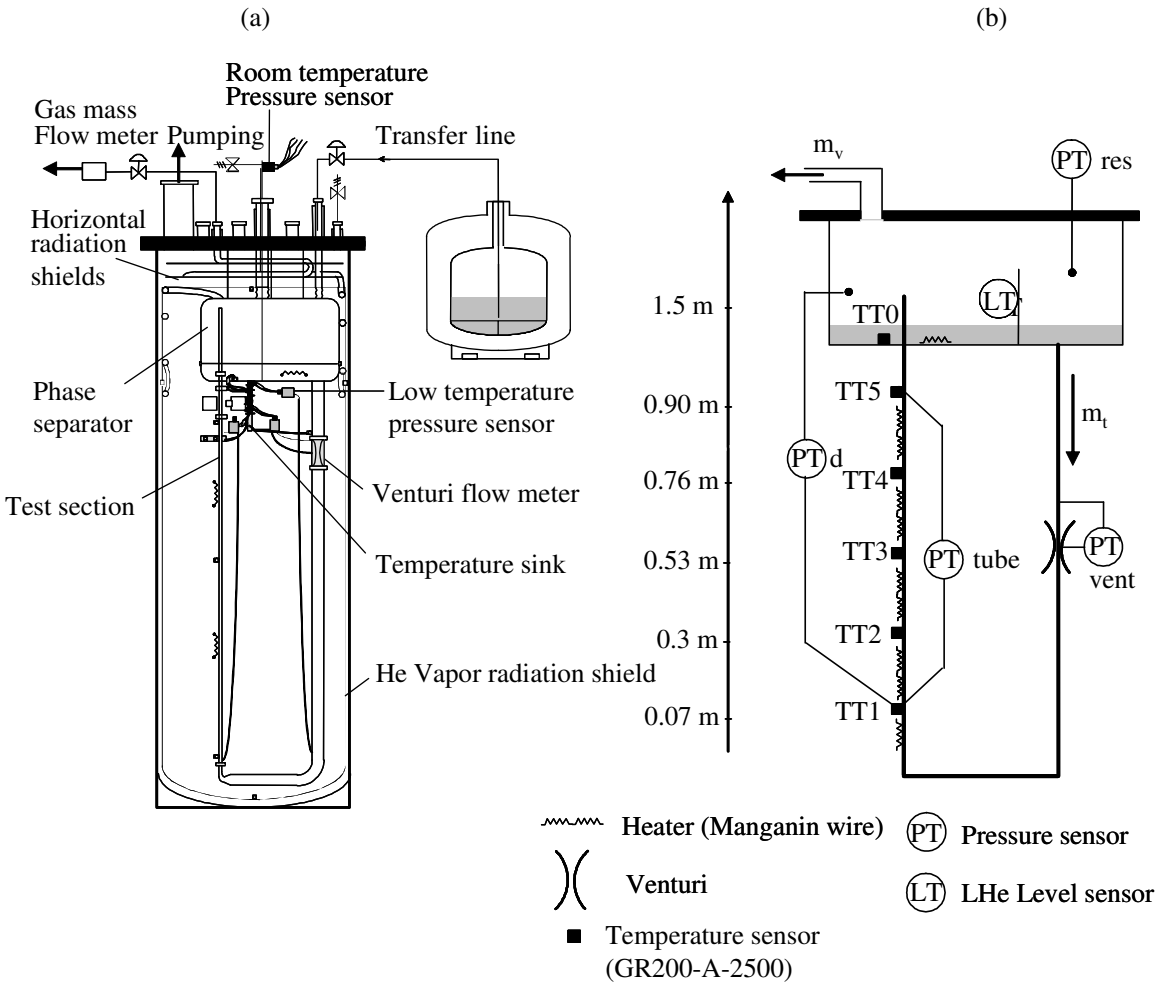

Figure. 1. Schematic of the experimental set-up: (a) cryostat overview and (b) thermosiphon loop.

($h=q/\Delta T$). These sensors have a sensitivity of 5×10^3 Ω/K allowing millikelvin measurement sensivity at 4.2 K and thermal response time of 200 ms. The temperature sensors are calibrated within 1 mK from a reference sensor, adding 1 mK, and the electronic chain adds another mK. The experimental uncertainty is maximize to 3 mK for temperature measurement but can lower for temperature difference measurement (2.8 mK) since the systematic error due to calibration can be retrieved when the difference from the measurement and the fitted curve has the same sign (most cases).They are inserted in small copper blocks brazed on the external surface of the tube. Thermometer wiring leads, made of phosphor bronze, are wrapped and glued around the copper blocks with GE varnish, and then attached to a temperature sink held at 4.2 K. This set-up reduces the conduction heat leaks through the wires arriving to the sensors down to μW level, and thus ensures that the measured temperature is that of the inside wall-temperature.

Two pressure taps with 2 mm diameter were drilled into the tube at either side of the heated length. The pressure taps are connected to a Yokogawa differential pressure transducer, PTtube, to measure the pressure drop along the heated test section. A second differential pressure gauge, PTd, has been installed between the phase separator and the inlet of the test section measuring the available driving head, ρgh. The pressure sensors have a 2 Pa sensitivity.

Furthermore, our experiment is equipped with two mass flow-meters, "a gas flow-meter" measuring the vapour mass flow rate $\dot{m}_v$ and "a Venturi flow-meter" measuring the liquid mass flow rate (*i.e.* total mass flow rate) $\dot{m}_t$ inside the downward tube. The gas flow-meter is located after a heat exchanger which heats He gas leaving the cryostat at ambient temperature. It is capable of measuring up to 4.2 g/s of He gas at room temperature with a precision of ± 0.01 g/s. The liquid mass flow-meter is a 0.4 m long Venturi with an entry inner diameter of 40 mm and a neck diameter

of 10 mm and it is placed in the downward tube. The precision of our mass flow rate measurement is about 10% of the measured value over the entire deposited power range.

2.2 Experimental Procedure

Before starting experiments, the thermosiphon loop is leak checked from the outside to ensure that the entire assembly is leak tight. The vacuum space around the experimental set-up is pumped down to 10^{-5} mbar and the outside thermal shield is filled with liquid nitrogen LN_2. The LN_2 level is regulated and allows the cryostat to cool down to 77 K overnight. Finally, liquid helium is transferred from the liquid storage dewar to the experimental loop through insulated transfer line. Transfer is stopped when the liquid level is about 25 cm in the separator. At this stage, experiments can be carried out as follows: after regulating the pressure above the liquid bath, heater located on the test section is energized. When steady-state conditions are reached, the measurement of the different parameters (total and vapour mass flow rates, temperatures, pressure drop, liquid level,…) are recorded by computer via a program through a multi channels data acquisition at 1 kHz per channels.

3 RESULTS AND DISCUSSION

3.1 Wall and fluid temperatures distribution

Fig. 2 depicts thermodynamic state evolution of He I flow subjected to heat flux and pressure variation through the loop on a *p-T* diagram. At state (1), phase separator is filled with atmospheric saturated He I (4.2 K). Due to liquid head H_1; liquid helium (LHe) enters at the bottom of the test section in a sub-cooled state, (2), and receives heat as it moves upward. To calculate the thermodynamic properties at state (2), we assume an isothermal compression process between states (1) and (2) since the value of H_1 is small compared to the system pressure (atmospheric pressure). The liquid temperature continues to increase and reach the saturation value of state (3). At this point, the saturated nucleate boiling regime begins with the existence of a net vapour generation resulting in two-phase flow region. Then, saturation temperature decreases due to channel pressure drop and reaches state (1).

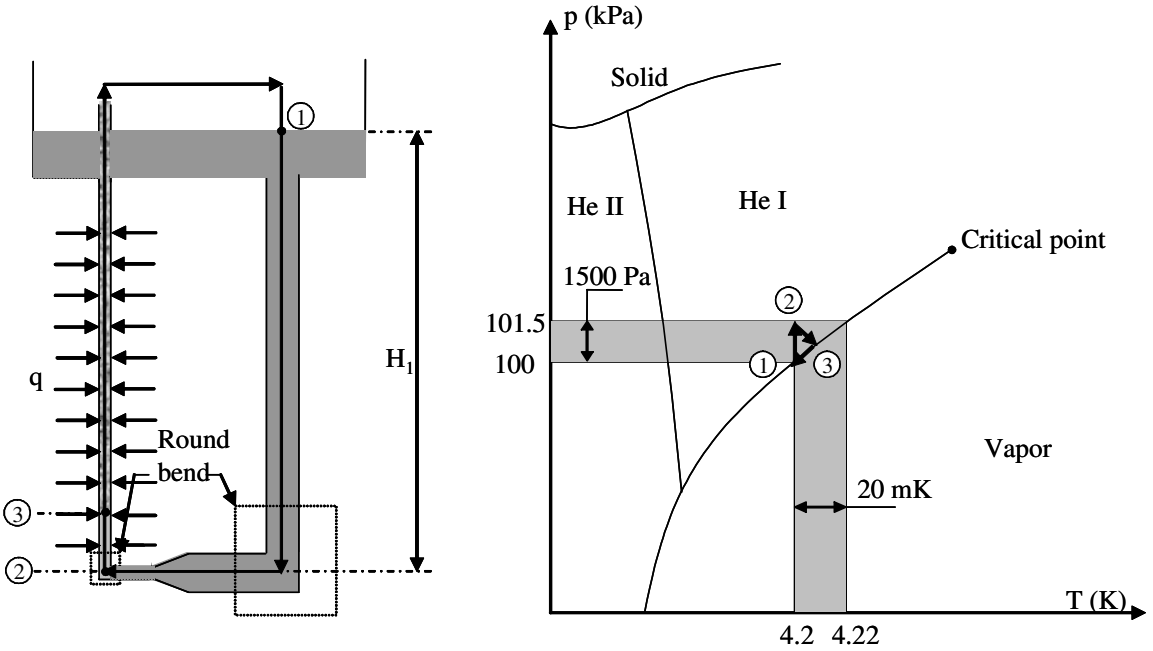

Figure. 2. p-T Domain of interest

The fluid temperature T_f in the sub-cooled region is computed from the energy balance equation while neglecting pressure and kinetic energy variations,

$$T_f = T_i + \frac{q\pi D - \dot{m}g}{\dot{m}C_{pf}} z_{sub}, \tag{3}$$

where T_i is the liquid inlet temperature, and z_{sub} the length of the sub-cooled region determined iteratively by using the HEPAK code [16]. In the two-phase region, T_f is the fluid saturation temperature corresponding to the pressure at a given channel height z determined from PTd and PTres measurements (Fig. 1(b)).

Typical plots of wall and fluid temperatures distribution along the heated length of the test section as a function of heat flux are given in Fig. 3. The wall temperature, T_w, rises along the heated length of the tube from the inlet up to a maximum temperature beyond which a steep fall sets in. As for other mixtures, the decrease in the wall temperature is due to the apparition of nucleate boiling which comes into play in addition to the forced convection process [17, 18]. In the entrance region, the liquid temperature, T_f, increases up to the saturation point, then, a very slight decrease in the saturation temperature as a result of pressure drop is observed [17, 18].

3.2 Mass flow rate and vapour quality

As mentioned above, vapour mass flow rate $\dot{m}_v$ is measured at the exit of the cryostat at room temperature and the total mass flow rate is given by the venturi flow-meter. Fig. 4 reports their evolution (a) and the resultant quality, $x = \dot{m}_v / \dot{m}_t$ (b), as a function of heat flux. Different points correspond to different experimental sessions performed each with an initial pressure of around 1 bar for the entire range of heat flux. Note that the scattering of the data gives a good representation of the experimental reproducibility. The experimental reproducibility of $\dot{m}_t$ is within ±10% at low q and ±5% at high q. For $\dot{m}_v$ the reproducibility is better at ±5%. Before heater is turned on, the measured vapour mass flow rate of around 0.08 g/s gives an estimate of the cryostat heat leakage (1.7 W). It represents a systematic error for measurements and is deduced from $\dot{m}_v$ data for each applied heat flux. Fig. 4(a) shows that the total mass flow rate increases rapidly with heat flux up to a value of 10 g/s in the range of q between 0 and 500 W/m^2. In this region, the gravitational pressure drop in the heated section is dominant and it decreases with the void fraction, and thus $\dot{m}_t$ rises with heat flux. On the other hand, in the high heat flux region, the frictional pressure drop becomes preponderant and increases with void fraction. Thus, $\dot{m}_t$ decreases with increasing heat flux. In such a region, we indeed observe a small diminution above 2000 W/m^2.

The vapour quality, x, is defined as the ratio between the vapour mass flow rate, $\dot{m}_v$, and the total mass flow rate, $\dot{m}_t$. Theoretically, the exit quality can be computed using the energy balance equation integrated over the two-phase flow region. Thus, the equation for x is:

$$\dot{m}_t\left(i_f(z) - i_f(z_{sub})\right) + \dot{m}_t L_v(z)x + \frac{8\dot{m}_t^3}{\pi^2 D^4 \rho_f^2}\left[\frac{x^3\rho_f^2}{\alpha^2\rho_v^2} + \frac{(1-x)^3}{(1-\alpha)^2} - 1\right] + \dot{m}_t g\left(z - z_{sub}\right), \tag{4}$$
$$= q\pi D\left(z - z_{sub}\right)$$

where i_f is the enthalpy of the liquid phase, α the void fraction calculated from the homogeneous model, and z the channel height. The solution of Eq. (4) is depicted on Fig. 4(b) as a solid line. The vapour quality predicted by Eq. (4) is always higher than our measurement. It is 10% higher than the experimental data up to 1000 W/m^2. For higher heat flux the discrepancy can be as high as 30%. The tests are performed with a variable liquid level in the phase separator since transferring permanently liquid helium in the reservoir to maintain a constant level increases the vapour mass flow rate so that the identification of $\dot{m}_v$ becomes difficult and leads to large experimental errors.

But the fraction of vapour remaining inside the phase separator to compensate the liquid level diminution, reducing the vapour mass flow rate measurements, is small. It is typically in the order of 0.1 g/s. In fact, we attribute the discrepancy between the date and Eq. (4) to the use of the homogeneous model which becomes inaccurate to model our data above q=1000 W/m^2 where boiling crisis occurs.

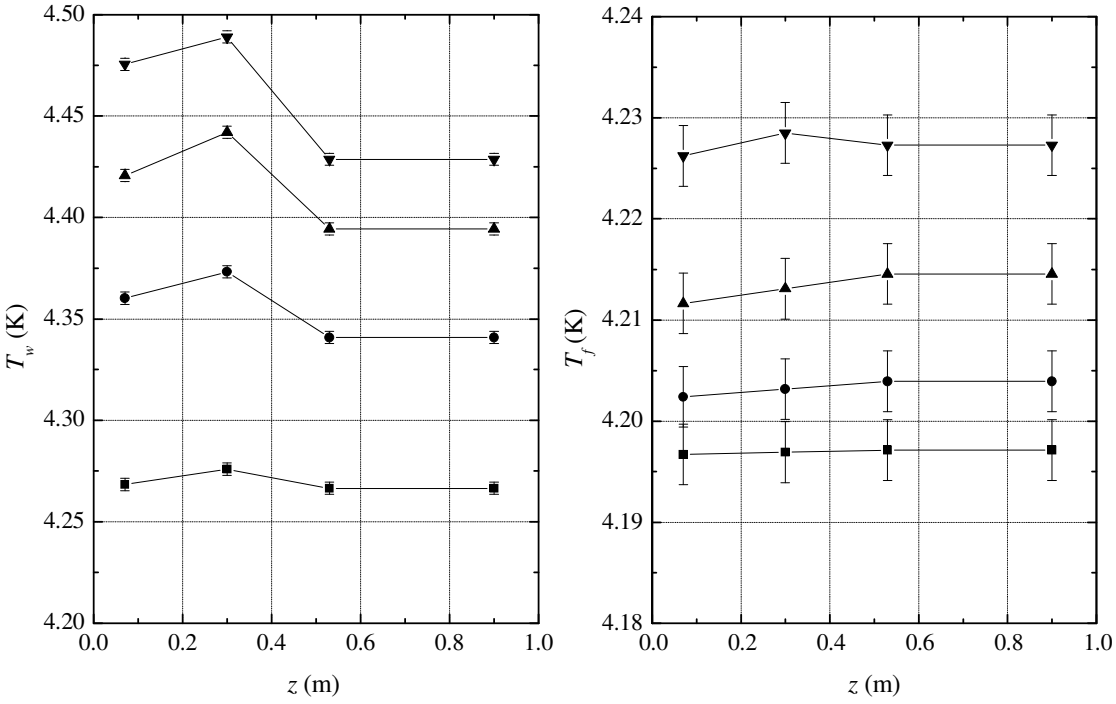

Figure 3. Variation of wall and fluid temperatures along the heated length for different heat flux. ■: q=100.23 W/m^2, ●: q=501.92 W/m^2, ▲: q=1004.47 W/m^2, ▼: q=1605.56 W/m^2.

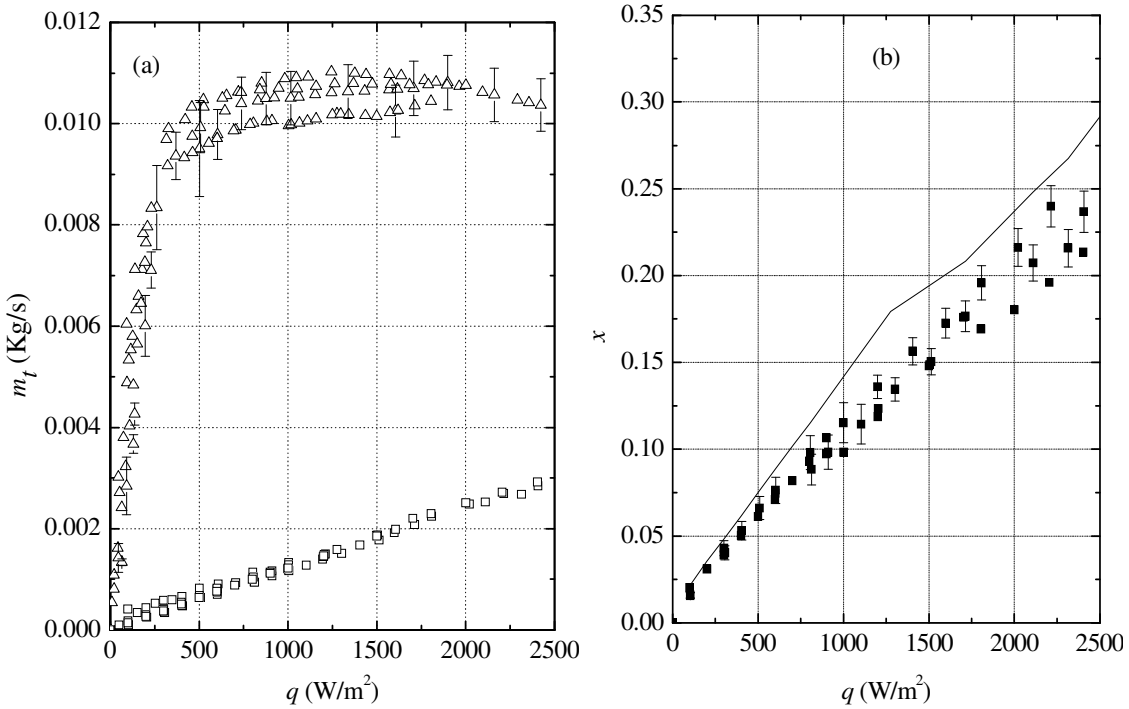

Figure. 4. (a) Vapour and total mass flow rates, Δ: $\dot{m}_t$, □: $\dot{m}_v$ and (b) exit quality x as a function of heat flux. Error bars are partially presented for clarity. The error bars of $\dot{m}_v$ are of the size of the symbols.

3.3 Boiling curves

Fig. 5 presents typical traces of the obtained boiling curves *i.e*. the measured wall superheat, ΔT_w which is the difference between the wall temperature, T_w, and the fluid temperature, T_f versus heat flux at 0.07 m and 0.3 m channel height. The overall characteristics of the curves may be described as follows. At low heat flux, one can see that the evolution of the temperature difference is linear. It is well known that a linear relationship between the wall superheat and the heat flux reflects that the heat is removed by single-phase forced flow. In this region for a given heat flux, wall superheat increases towards the tube exit indicating the dependence of the channel height on the heat transfer coefficient. The heat transfer at the entrance of the tube is enhanced because the flow is under development [19]. Note also that the sub-cooled boiling could improve the heat exchange in this region but we are unable to visualize it. Anyhow, the following analysis demonstrates that if any subcooled boiling occurs, its effect is negligible.

The single phase liquid forced convection region (SPL) has been predicted by Taine and Petit's correlation [19]:

$$h_{CV} = 0.023\, Re_f^{\,0.8}\, Pr_f^{\,0.4} \left(\frac{\lambda_f}{D}\right)\left(1+6\frac{D}{z}\right), \tag{5}$$

where λ_f is the liquid thermal conductivity, Pr_f the liquid Prandtl number, and Re_f the liquid Reynolds number based on the total mass flow rate. One can see in Fig. 5 that Eq. (5) follows our results in the low q region within 8% accuracy. The good agreement between the Taine and Petit's correlation and our data grants the use of Eq. (5) to identify the single phase region.

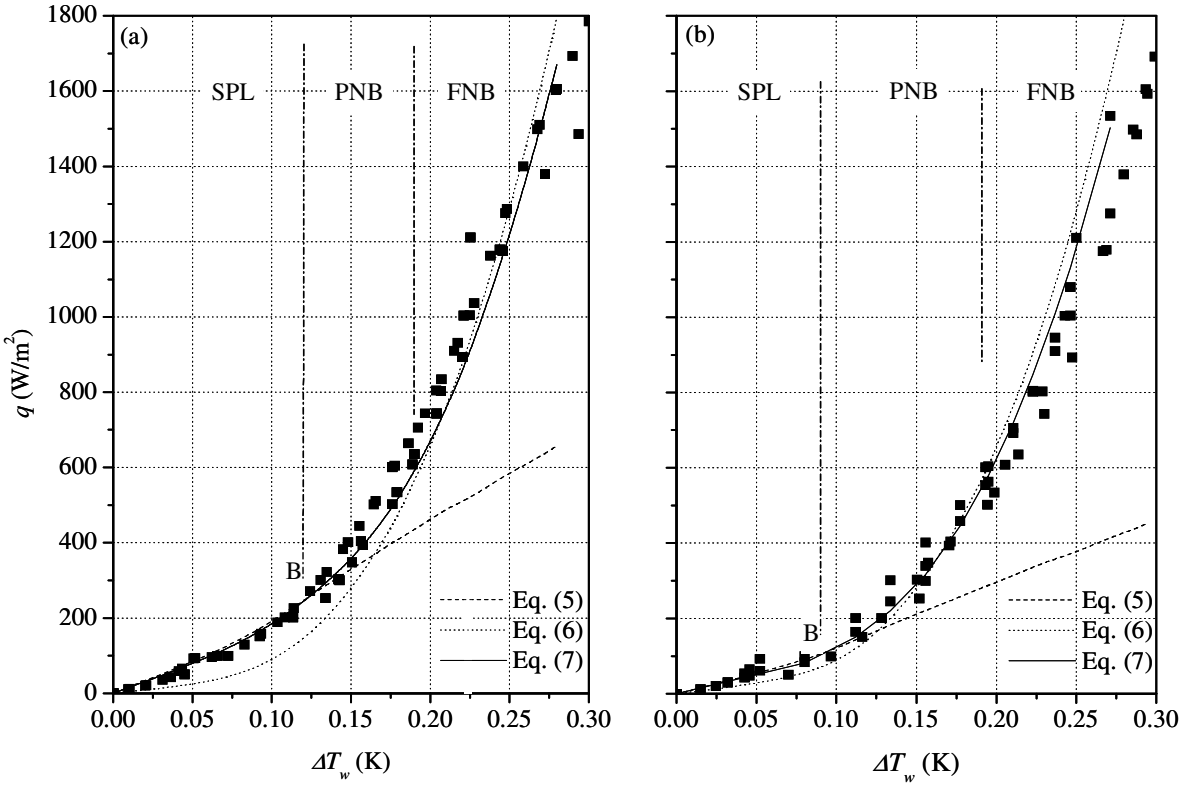

Figure. 5. Boiling Curves at (a) z=0.07 m and (b) z=0.3 m channel height predicted by Eq. (8) using our nucleate boiling flow data. Error bars are of the size of the symbols.

As the heat flux increases, the wall temperature rises until a threshold value where nucleation cavities are activated. Boiling incipience manifests itself by an increase in the slope curve dq/dΔT. It occurs first towards the exit of the heated section, and with increasing heat flux, the point of boiling

incipience shifts towards the tube inlet. In our experiments, the boiling incipience ΔT_w corresponds to the point B on Fig. 5. It is around 0.11 K for z=0.07 m, 0.08 K for z=0.3 m. These values are 10 times greater than those predicted by the Graham and Hsu theory [20]. This is presumably because the process of bubble nucleation is affected by the induced flow. With increasing mass flow rate, the thermal boundary layer becomes thinner, and the linear temperature gradient within it is not sufficient to allow bubble formation, thus nucleation is delayed [17].

After the point B, boiling curve deviates from the single-phase line given by Eq. (5) indicating heat transfer enhancement by nucleate boiling. The heat transfer in the partial nucleate boiling region is dominated basically by two effects: the macro-convection due to the motion of the bulk liquid and micro-convection induced by departing bubbles from the wall.

At high heat flux, more and more nucleation sites are activated and the heat flux steeply increases with the wall temperature difference representing the fully developed nucleate boiling (FNB) region. In this zone, the wall is completely covered with bubbles and the bulk flow velocity influence becomes less and less important and the nucleate boiling mechanism prevails. The wall superheat is independent of the channel height and depends on heat flux, pressure and surface characteristics [18]. A typical relationship used to fit the data in the (FNB) region is:

$$q = \psi.\left(T_w - T_{sat}\right)^m, \tag{6}$$

where T_w is the wall temperature, T_{sat} the saturation temperature, and ψ a parameter containing the effect of pressure, physical properties and the wetting characteristics of surface-fluid combination. m ranges from 2 to 4 in various published correlations. In this study, the best fit using Eq. (6) for fully developed nucleate boiling data was obtained for m=3 and ψ=82000 W/m^2.K^3 for the entire FNB region and for any height within 10% accuracy.

3.4 Proposed model and comparison

The two-phase heat transfer coefficient can be modelled by the power law (Eq. (2)):

$$h_{TP} = \left(h_{CV}{}^3 + h_{EN}{}^3\right)^{1/3}, \tag{7}$$

where h_{CV} is given by the Taine and Petit's correlation (Eq. (5)) and h_{EN} is given by Eq. (6) as $h_{EN} = \psi^3 q^{2/3}$. Choosing F=1, S=1 and 3 as an exponent in Eq. (7) yields the best prediction of our experimental data especially in the transition region. It was found that higher values of n predict a higher heat transfer coefficient with a sudden transition while lower n values predict a lower value, extending the transition range. The entire boiling curves at z=0.07 m and z=0.3 m are predicted by Eq. (7) as Fig. 5 shows, where the transition region is fitted within 10% accuracy. One can see that boiling curves merge with the forced convection curve at low wall superheat and with the fully developed boiling curve at relatively high wall superheat.

Among various existing heat transfer correlations for saturated boiling flow available in the literature, three are frequently referenced: Chen's correlation (n=1), Liu-Winterton's (n=2) and Steiner-Taboreck's (n=3). In Fig. 6, a comparison between them and our model given by Eq. (7) is reported. On average our model gives an accuracy of 12%, the best among the tested correlations. The second is Steiner-Taboreck model with 25% followed subsequently by the Liu-Winterton with 28% and the Chen with 40% finally. The tested correlations originally developed in forced flow environments under-estimate our heat transfer coefficient data. This is due to the fact that the flow in thermosiphon loop is always under development.

3.5 Boiling crisis and critical heat flux

Plotted on Fig. 7 is heat flux against wall superheat at the entrance (z/D=7) and at the exit (z/D=90) of the test section. For clarity, we present here only two sets of data that are representative of the experimental reproducibility. One can see the drastic rise in ΔT_w (around 3 K) associated to the boiling crisis occurring when the heated surface is covered with a vapour film as the result of intensive boiling. The maximum heat flux just before boiling crisis corresponds to the critical heat

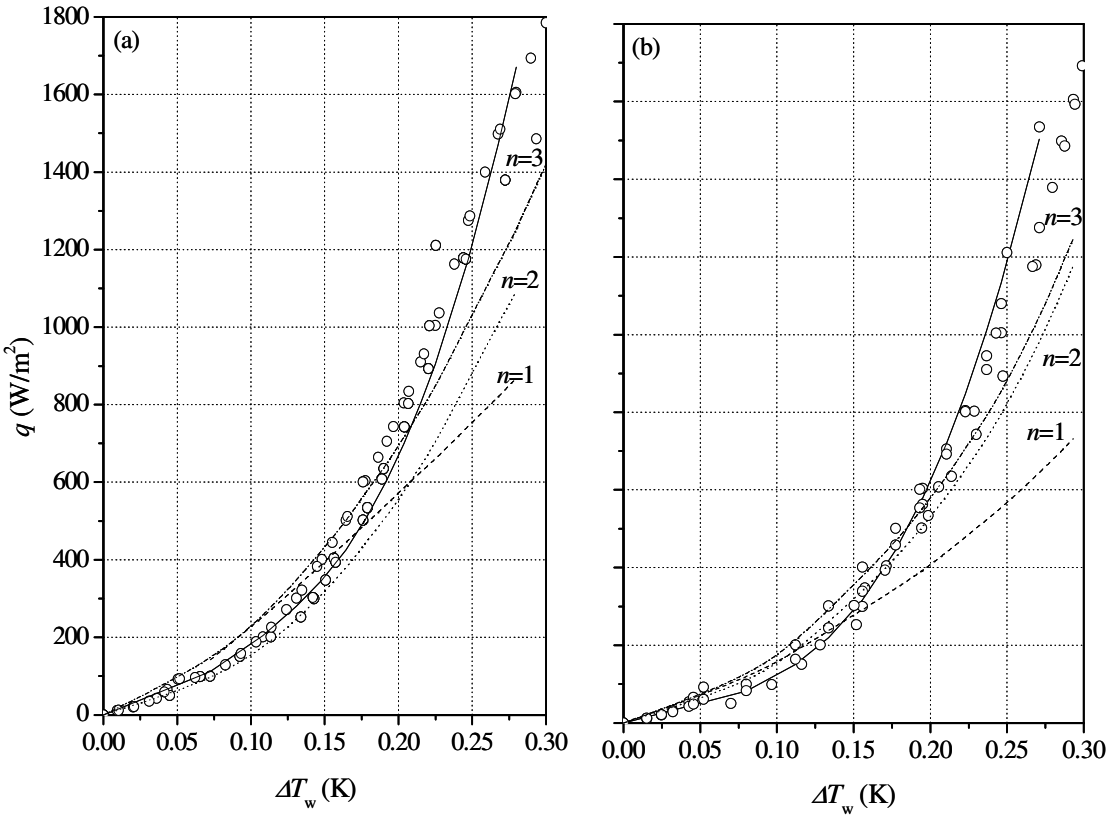

Figure. 6. Comparison of prediction boiling curves with different correlations at (a) z=0.07 m and (b) z=0.3 m channel height. ○ Experimental data, Chen's model, Liu-Winterton model, Steiner's model, and the proposed model. Error bars are of the size of the symbols.

flux (CHF), q_{cr}. For our experiments, q_{cr} ranges from 1500 W/m^2 to 2000 W/m^2 and have been determined within 50 W/m^2. These CHF values are about 35% of those measured by Lyon [21] under pool boiling conditions on a horizontal flat plate. It is due to the buoyancy effect which decreases as the surface is turned from horizontal to vertical orientation.We also remark that the onset of boiling crisis occurs first at the exit end of the heated section where the vapour quality is the highest and as heat flux is increased, it propagates towards the inlet of the tube.

Calculating CHF is of great importance in the design of heat exchangers since exceeding the CHF leads to a drastic reduction of the heat transfer coefficient, causing a system dysfunction. For this reason, numerous studies have been realized to predict CHF in both natural and forced convection systems under different conditions.

For natural flow configuration, Katto and Kawamura [22], Monde and Yamaji [23] and Monde and Mitsutake [24] conducted several experiments and proposed empirical correlations for vertical round tubes. The correlations are based on the Kutateladze number and on the ratio between the tube length and the hydraulic equivalent diameter. They can be generally expressed as follows:

$$Ku = \frac{q_{cr}}{\sqrt{\rho_v} L_v \sqrt[4]{\sigma g \left(\rho_f - \rho_v\right)}} = \frac{A}{B + C\left(z/D\right)}, \tag{8}$$

where Ku is the Kutateladze number and A, B, and C are experimental constants which varied widely from a study to another. Eq. (8) is a simple modification of the well known correlations developed for pool boiling with the effect of the channel aspect ratio z/D.

For forced flow configuration, correlations have been established. Based on large data bank including cryogenic fluids (Helium, Nitrogen,…), Katto [25] proposed the following functional form to correlate flow boiling CHF data for uniformly heated tubes:

$$q_{cr} = f\left(\frac{\rho_v}{\rho_f}, We_f, \frac{L}{D}\right)\left(1 + \frac{K \Delta h_{sub}}{L_v}\right), \tag{9}$$

where We_f is the Weber number, Δh_{sub} the subcooled enthalpy and K an empirical coefficient depending on the flow regime. For the present analysis, we use f and K values recommended for He in [25].

Shah [26] built a general correlation for CHF for subcooled and saturated flow boiling in vertical tubes. It was elaborated using a wide data base of different fluids (water, halocarbon, refrigerants, chemical, liquid metals, helium and other cryogens). It consists of two correlations, one concerned with a situation where CHF is function of the upstream conditions (UCC), e.g., inlet subcooling and distance from tube inlet and the other where CHF depends only on local quality (LCC). The correlation is:

$$\frac{q_{cr}}{GL_v} = f(\frac{L}{D}, Y, x_i) \text{ for the UCC and } \frac{q_{cr}}{GL_v} = f(\frac{L}{D}, Y, x_e, p_r) \text{ for the LCC}, \qquad (10)$$

where $Y = PeFr^{0.4}\left(\mu_f/\mu_v\right)^{0.6}$ is a dimensionless number. $Pe = GDC_{pf}/\lambda_f$ is the Peclet number, $Fr = G^2/\rho_f^2 gD$ is the Froude number and $p_r = p/p_c$ is the reduced pressure. For He, Shah recommends the use of UCC correlation [26].

Finally, few CHF correlations specific to He boiling flow are reported in literature. One can cite Lehongre *et al.* [27] for a natural circulation loop and Giarratano *et al.* [28] and Keilin *et al.* [29] for forced flow conditions. The latter two over-predict our data by a factor of 2~3 (Giarratano's correlation) and 4~6 (Keilin's). For that reason, they will not be discussed in the subsequent analysis.

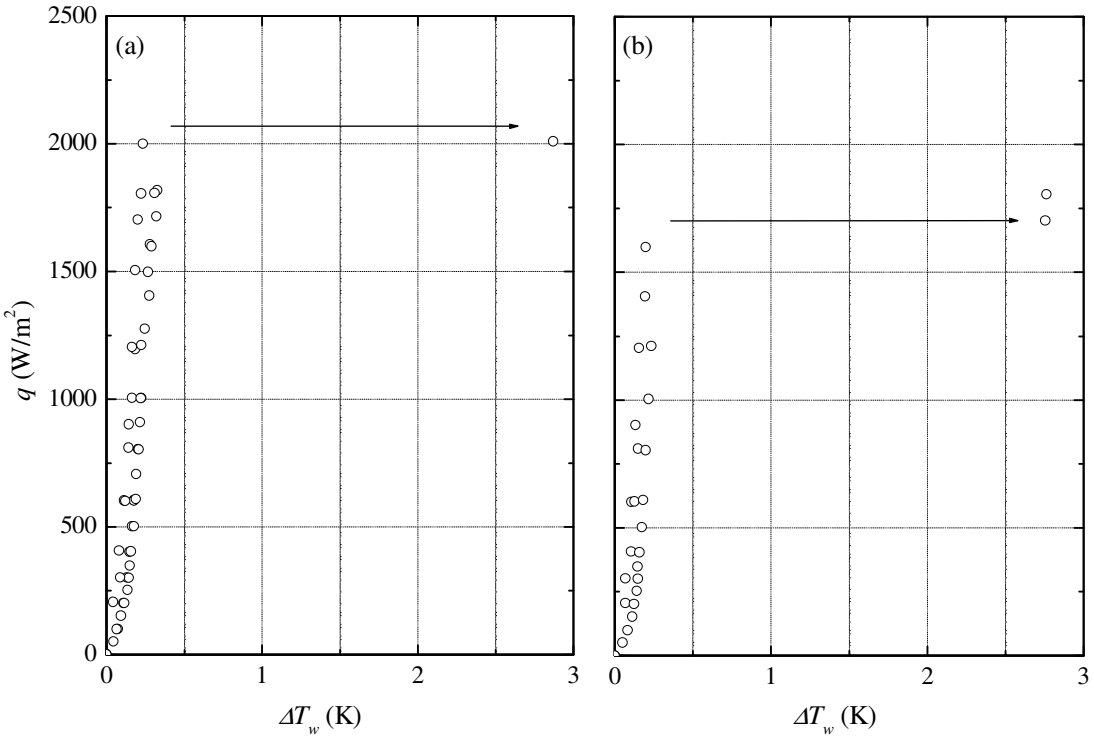

Figure. 7. Transition from nucleate boiling regime to film boiling regime at (a) *z/D*=7 and (b) *z/D*=90. Error bars are of the size of the symbols.

In Fig. 7, we present a comparison of our experimental CHF data with those of Lehongre, Katto, Shah, and Monde. For high *z/D* values, Lehongre's correlation predicts our data fairly well with a slight over-prediction. However, for low *z/D* our experimental data deviates from Lehongre's prediction. Although a relatively small disagreement for low *z/D*, Shah's and Katto's correlations give the best estimation among the tested ones. They predict our data within 20 and 30% respectively. This is expected since our flow parameters (mass flow rate, pressure, etc…) lie within the range covered by these correlations. A large disagreement from the prediction can be observed

for Monde's correlation, which is established for non-cryogenics fluids (water, ethanol, R113, and benzene). Finally, an attempt is made to correlate our experimental CHF data using Eq. (8). It predicts our results within a few percent with A=0.16, B=3.828±0.097 and C=0.01190±0.0019.

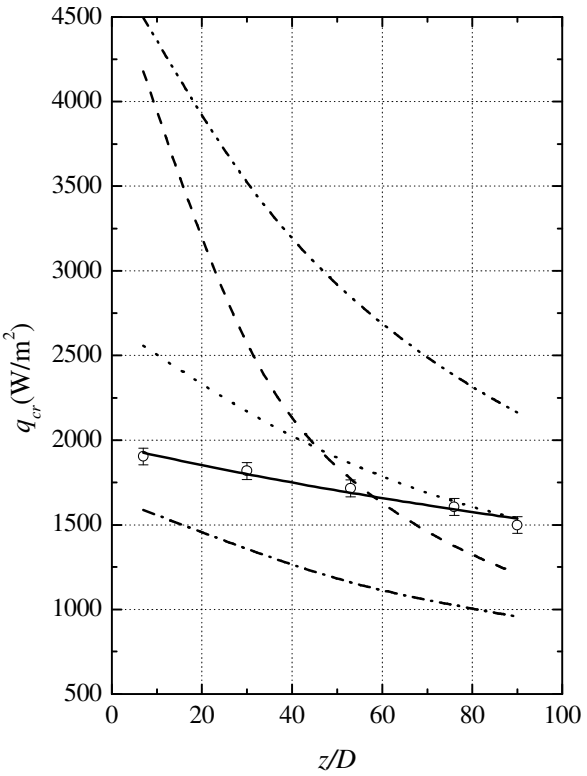

Figure. 8. Comparison between experimental data and the different correlations as *z/D*. ■ Experimental data, Monde's correlation, Lehongre's correlation, Katto's correlation, Shah's correlation, The proposed correlation.

4 CONCLUSION

The present paper investigates experimentally heat transfer characteristics of two-phase liquid helium (He I) in a natural circulation loop. The obtained boiling curves reveal the existence of three heat transfer regions: a single phase forced convection region, a partial nucleate boiling region and a fully developed nucleate boiling region. They are examined in detail to predict heat transfer coefficient along the whole boiling curve. A model combining the effect of forced convection and nucleate boiling heat transfer has been proposed. It reproduces the single phase forced convection in the low wall superheat region and the fully developed nucleate boiling in the high wall superheat zone. In the transition region both forced convection and nucleate boiling coexist and contribute to heat exchange. A comparative discussion between the most reliable models available in literature and our model indicates that our model gives the best estimate. Boiling crisis is reached in the range of heat flux from 1500 to 2000 W/m^2 where boiling curves exhibit a sharp increase in wall superheat of the order of 2 to 4 K. It appears first at the exit of the test section and shifts towards the inlet as the applied heat flux is increased. Prediction of experimental CHF data as a function of *z/D* ratio is carried out. Our results match within a few percent with this prediction.

ACKOWLEDGEMENT

This work was supported by the CERN-CEA collaboration for the construction of the 4T CMS magnet. The authors wish to thank Dr. F. Kircher and Dr. D. Campi for their financial support, Dr. Brédy for helpful discussions, H. Kabbouch, M. Cazanou and F. Paget for technical assistance.

REFERENCES

1. J.C. Lottin and F.-P. Juster, Liquid Helium Thermosiphon for the 4 Tesla CMS Solenoid, in Advances in Cryogenic Engineering, Plenum Press, 43, 1998, pp. 1505-1511.
2. Y. Zvirin, A review of natural circulation loops in pressurized water reactors and other systems, Nuclear Engineering and Design, 67 (1981) 203-225.
3. C. Johannes, Studies of forced convection heat transfer to helium I, in Advances in Cryogenic Engineering, Plenum Press, 17, 1972, pp. 352-360.
4. B. Baudouy, Heat and Mass Transfer in Two-phase He I Thermosiphon Flow, in Advances in Cryogenic Engineering, AIP, 47B, 2001, pp. 1514-1521.
5. B. Baudouy, Pressure drop in two-phase He I natural circulation loop at low vapor quality, in International Cryogenic Engineering Proceedings, edited by P. S. G. Gistau Baguer, Grenoble, France,19, 2002, pp. 817-820.
6. W.M. Rohsenow and B.B. Clarck, A new correlation of pool boiling data including the effect of heating surface characteristics, Journal Heat Transfer, 1969) 245-250.
7. F.W. Dittus and L.M.K. Boelter, Heat transfer in automobile radiators of the tubular type, University of california publications in engineering, 2 (1930) 443-461.
8. W.M. Rohsenow, A method of correlating heat transfer data for surface boiling of liquids, Journal Heat Transfer, 74 (1952) 969-976.
9. A.E. Bergles and W.M. Rohsenow, The determination of forced-convection surface boiling heat transfer, Journal Heat Transfer, 86 (1964) 365-372.
10. J.C. Chen, A correlation for boiling heat transfer to saturated fluids in convective flow, Ind Engng Chem. Proc. Des. Dev, 5 (1966) 322-329.
11. M.M. Shah, A new correlation for heat transfer during boiling flow through pipes, ASHRAE Trans., 82 (1976) 66-86.
12. K.E. Gungor and R.H.S. Winterton, A general correlation for flow boiling in tubes and annuli, International Journal of Heat and Mass Transfer, 29 (1986) 351-358.
13. Z. Liu, Winterton, R.H.S., A general correlation for saturated and subcooled flow boiling in tubes and annuli based on a nucleate pool boiling equation, International Journal of Heat and Mass Transfer, 34 (1991) pp. 2759-2766.
14. S.G. Kandlikar, A general correlation for saturated two-phase flow boiling heat transfer inside horizontal and vertical tubes, Journal Heat Transfer, 112 (1990) 219-228.
15. D. Steiner and J. Taborek, Flow boiling heat transfer in vertical tubes correlated by an assymptotic model, Heat Transfer Engng, 13 (2) (1992) 43-69.
16. Cryodata, HEPAK Helium Properties v. 3.4, 1999
17. J.G. Collier and J.R. Thome, Convective Boiling and Condensation, 3rd Ed ed., O.U. Press, Oxford, 1994.
18. L.S. Tong, Tang, Y.S., Boiling heat transfer and two-phase flow, 2nd ed., T. Francis, 1997.
19. J. Taine and J.-P. Petit, Transferts Thermiques - Mécanique des Fluides Anisothermes, 1989.
20. Y.-Y. Hsu and R.W. Graham, An analytical and experimental study of the thermal boundary layer & ebullition cycle in nucleate boiling. 1961, Lewis Res. Ctr., Cleveland,OH.
21. D.N. Lyon, Heat transfer and peak nucleate boiling fluxes in saturated liquid helium between in Advances in Cryogenic Engineering, 10, 1965, pp. 371-378.
22. Y. Katto and S. Kawamura, Critical heat flux during natural convective boiling in vertical uniformly heated tubes submerged in saturated liquid, Journal Heat Transfer, 47 (1981) 2186-2190.
23. M. Monde and K. Yamaji, Critical heat flux during natural convective boiling in a vertical uniformly heated tubes submerged in saturated liquid, Journal Heat Transfer, 112 (1990) 111-116.
24. M. Monde, Y. Mitsutake, and M. Hayashi, Critical heat flux during natural convective boiling in a vertical tube: effect of oscillation and circulation on CHF, International Journal of Heat and Mass Transfer, 45 (1999) 4133-4139.
25. Y. Katto, A generalized correlation of critical heat flux for the forced convection boiling in vertical uniformly heated round tubes, International Journal of Heat and Mass Transfer, 21 (1978) 1527-1542.
26. M.M. Shah, Improved general correlation for critical heat flux during upflow in uniformly heated vertical tubes, International Journal of Heat and Fluid Flow, 8 (1987) 326-335.
27. S. Lehongre, et al., Critical nucleate boiling of liquid helium in narrow tubes and annuli, in International Cryogenic Conference Proceedings, Ilife Science, 2, 1968, pp. 274-275.
28. P.J. Giarrantano, R.C. Hess, and M.C. Jones, Forced convection heat transfer to subcritical helium I, in Advances in Cryogenic Engineering, Plenum Press, 19, 1974, pp. 404-416.
29. V.E. Keilin, V.V. Likov, and M.M. Pozvonkov, Forced convection heat transfer to liquid helium I in the nucleate boiling regim region, Cryogenics, 15 (March) (1975) 141-145.